OPTICAL EVALUATION OF 3D PRINTED CPC BY COUPLING PHOTOGRAMMETRY AND RAY TRACING ANALYSIS

Pedro R. Martínez-Manuel[1], Luis M. Valentín-Coronado[2], Iván Salgado-Transito[2], Manuel I. Peña-Cruz[2], Fernando Martell-Chávez[3], J. Gonzalo Carrillo-Baeza[4], Carlos A. Pineda-Arellano[2]*

[1] Posgrado Interinstitucional de Ciencia y Tecnología – Centro de Investigaciones en Óptica, A.C. Unidad Aguascalientes, Prol. Constitución 607 Fracc. Reserva Loma Bonita, CP 20200 Aguascalientes, Aguascalientes, México
[2] CONACYT – Centro de Investigaciones en Óptica, A.C. Unidad Aguascalientes, Prol. Constitución 607, Fracc. Reserva Loma Bonita, CP 20200 Aguascalientes, Aguascalientes, México
[3] Centro de Investigaciones en Óptica, A.C. Unidad Aguascalientes, Prol. Constitución 607, Fracc. Reserva Loma Bonita, CP 20200 Aguascalientes, Aguascalientes, México
[4] Centro de Investigación Científica de Yucatán, Unidad de Materiales, Calle 43 No. 130 x 32 y 34, Chuburná de Hidalgo, CP 97205 Mérida, Yucatán, México

* capia@cio.mx

Manufacturing methods of CPC collectors, regardless the application, have not undergone significant modifications in recent years; the main manufacturing methods are hydraulic press stamping and some other machining methods, which generate errors in geometric curvature and damage to the high-reflectivity film coating, reducing the overall optical efficiency of the CPC. In this work, we propose a method for the fabrication of cylindrical CPCs (widely used in water-heating, disinfection, and wastewater treatment applications), which comprises the use of a 3D printed mold complemented with a structural styrofoam molding. The proposed method presents the advantage of improving the quality of the CPC profile with less damage on the surface of the high reflectivity coating and with a reduction in the quantity of deformations because of its machining processes. To evaluate the effectiveness of the presented method, an experimental-simulation test was carried out based on a photogrammetric technique combined with a Ray tracing Monte Carlo method. The test procedure compared the CPC manufactured with the proposed method (called 3DM-CPC) versus one manufactured by a conventional machining technique (referred as CM-CPC). The results obtained show a geometrical mean error value of 1.2 mm for the 3DM-CPC compared to 3.19 mm for the CM-CPC. Optical assessment by ray tracing showed a relative efficiency of 95% for the 3DM-CPC versus 82% of the CM-CPC, both of them compared to the theoretical ideal geometry of a 2D-1 Sun CPC. The benefit could be estimated in a simulation to be 9.4% in the annual performance of a 1000 L CPC thermal energy solar plant.

Keywords: CPC manufacturing, 3D printed molds, photogrammetric technique, photocatalytic reactor, solar concentrator

1 INTRODUCTION

Compound Parabolic Concentrators (CPC's) are non-image concentrators composed of parabolic reflectors that conduct solar radiation from the aperture area to the absorber. CPCs are widely used in many solar applications [1] such as photovoltaics [2], thermal [3], [4], daylighting [5], water detoxification and disinfection [6], [7], among others [8], [9]. This is because of their high optical efficiency, no-solar tracking system requirement at low solar concentration and their ability to capture both direct and diffuse solar radiation. Two key CPCs design parameters are concentration (C) and acceptance half-angle (θ_a), which are related by: $C = 1/sin(\theta_a)$. The concentration is the ratio of aperture to absorber area, while half-angle is the angle between the line of the edge of the parabola and the axis of symmetry. CPCs have the optical property that all rays incident on the aperture area within acceptance angle will reach the absorber, whereas all the rays with an angle of incidence greater than θ_a will bounce off the reflector and get lost off the aperture area.

The two-dimensional concentrator with cylindrical absorber is a particular type of CPC very useful for working with fluids. A popular geometry is the special case when θ_a= 90°, so the Concentration Ratio (CR) is equal to 1 Sun [10]; in which, if an ideal surface is considered, all the solar radiation that reaches the aperture is reflected towards the receiver tube. The CPC reflector is usually made of silver metallic foil-polymer or high specular reflectivity aluminum sheets [11], while the absorber is made of transparent glass or copper tubes depending on the application.

However, despite innovative changes in the geometric configurations of CPCs collectors for diverse applications, their manufacturing methods have not undergone significant modifications in recent years. The main manufacturing methods are lamination with a hydraulic press and by other machining methods, which generate errors in geometry and damage the high-reflectivity film, reducing the overall optical efficiency of the CPC. Recently, Carrillo et al. [12] developed a methodology to manufacture 2D cylindrical CPCs collectors using a Styrofoam mold cut by hot-wire technique, obtaining in this way the required shape without using mechanical fasteners. The performance results were analyzed by a photogrammetric technique.

In some studies, the thermal efficiency is investigated from the perspective of the support structure, design and construction where a frame of support ribs is used for its setting [13]. Other studies [14], use assemblies that required

joints which generate gaps between them. To reduce weight, they use light concrete shells as support structure instead of the steel frames, which provide stiffness and fill the gap between the supporting structure and reflecting surface. A study presented by Meiser et al. focused to investigate the deviation that occurs by the gravity load on the mirror shape and to study the deformation of the mirror because of gravity load and mounting forces and its effect on the shape of the mirror [15]. Balghouthi et al. studied the optical and thermal performance of a parabolic trough solar collector (PTSC) by photogrammetric techniques [16]. Besides, Osório et al. propose a method for customized design of a tracking CPC-type solar collector to minimize the energy cost[17], their results are based on the simulated ideal collector, discarding in this way, the fabrication bending or malformations that may affect the real performance. Atul S. Jadhav et al. [18] studied this factor that implies an energy loss of 17% in a low cost CPC system.

There are several methods to evaluate the collector's surface. Either by using pattern reflection deflectometry [19] or photogrammetry technique [20]; where Waghmare and Gulhane [21] found that the spread of reflected rays in the studied CPC increased because of manufacturing errors. Even using geometries mathematically defined and converted into CAD 3D models to be simulated with ray-tracing for estimating the flux distribution [22]. So, either one of these methods is effective depending on the particular purpose of the evaluation test.

In this context, to improve the optical efficiency of 2D cylindrical CPCs, this paper presents a manufacturing method that employs a 3D printed mold with the shape of the required CPC profile. Subsequently, a matrix is formed with the CPC mold, a drawer and a high reflectivity aluminum sheet. The polyurethane is injected into the cavity and waiting a time until the solidification reaction is completed. In the solidification process, the polyurethane expands and compresses the aluminum foil against the CPC mold and acquired the designed profile of the CPC. To evaluate the improvement in the geometry and optical efficiency of the CPC manufactured by the herein proposed method, a hybrid test was implemented using photogrammetry and ray tracing. Experimentally, the shape of the CPCs profile was characterized by photogrammetry. With this information, the shape of the entire CPC was reconstructed and a 3D model of the geometry was generated with CAD software. Subsequently, the geometry was exported to the Tonatiuh software and a ray tracing simulation was carried out to determine the optical efficiency.

2 MATERIALS AND METHODS

The presented method to manufacture the collectors using the 3D printed mold comprises two stages. The first one is about the design, 3D printing and construction of the CPC. The second one describes the evaluation made to the collectors to verify the manufacturing process by calculating their optical efficiency using Monte Carlo ray tracing.

2.1 CPC design

The design is performed using equations 1 and 2 for the involute shape and equations 3 and 4 for the parabola profile on a xy plane, where r is the external radius of the receiving tube, the rim angle φ is the angle between the axis and a tangential line from the focus to the physical edge of the concentrator. In the especial case where $\theta_a = 90°$ just the merely involute is schemed (blue line in Fig. 1) since there is no macrofocal parabola for the collector. Finally, θ_a is the half acceptance angle of the collector [23]. Fig. 1 shows the design for the CPC of $CR = 1\ sun$ for a tube with $r = 16.1\ mm$, CR is given by equation 5 where an angle of 90° was defined.

$$x = r\ (\sin\varphi - \varphi\cos\varphi) \tag{1}$$

$$y = -r\ (\varphi\sin\varphi + \cos\varphi) \tag{2}$$

$$\text{with } 0 \leq \varphi \leq \pi/2 + \theta_a$$

$$x_2 = r\ (\sin\varphi - A\cos\varphi) \tag{3}$$

$$y_2 = -r\ (A\sin\varphi + \cos\varphi) \tag{4}$$

$$\text{where } A = \frac{\left[\frac{\pi}{2} + \theta_a + \varphi - \cos(\varphi - \theta_a)\right]}{1 + \sin(\varphi - \theta_a)} \text{ with } \frac{\pi}{2} + \theta_a \leq \varphi \leq \frac{3\pi}{2} - \theta_a$$

$$CR = \frac{1}{\sin\theta_a} \tag{5}$$

2.2 3D printing and software tools

From the 2D generated involute, the 3D parabolic design that serves as a mold for the CPC is obtained. For this activity, AutoCAD® 2019 was used where the 2D involute is converted into a 3D mold of the collector. The design of the mold was made in 4 assembled parts (male-female), each piece has dimensions of 99.4 x 330 x 40.9 mm (limited to the 3D printing parameters), and thus reach the length required to cover the entire CPC receiver tube (1320 mm) used commonly in a photocatalytic reactor (low concentration e.g. 1-Sun). The mold manufacturing process was carried out in the 3D printer (ADEN®), with a 1.75 mm PLA filament thickness. The highly reflective aluminum sheet takes the geometric shape of the printed mold. In addition, a steel container was developed. This container has internal dimensions of 1320 x 102 x 50 mm, with a wall thickness of 5 mm. The mold container provides the adequate

Journal of Applied Engineering Science

Vol. 20, No. 4, 2022
www.engineeringscience.rs

iipp
publishing

Pedro R. Martínez-Manuel et al. - Optical evaluation of 3D printed CPC by coupling photogrammetry and ray tracing analysis

setting to maintain the mold and the aluminum sheet together under tension, causing the latter to take the form of the designed CPC
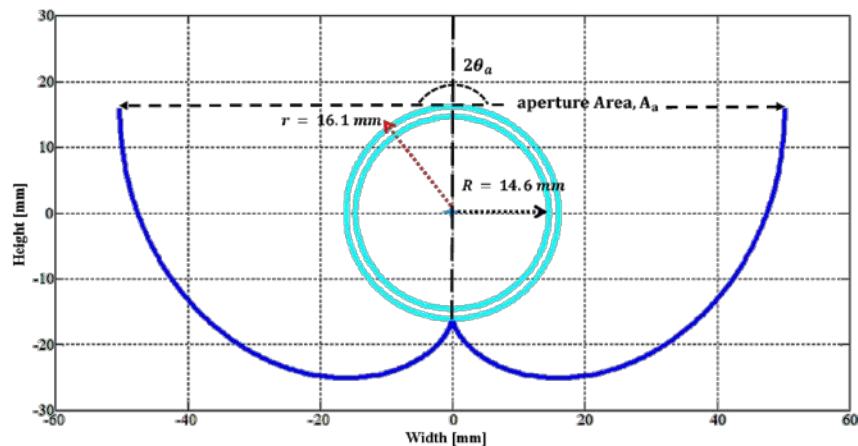

Fig. 1. Ideal 1-sun CPC design for a 32 mm glass tube diameter.

2.3   Polyurethane foam

In order to get the appropriate folding of the CPC laminate, liquid polyurethane foam was added into the container with the aluminum foil and the mold previously placed. The liquid polyurethane fulfills the function of exerting pressure on the reflective sheet against the mold as it expands throughout the container, thus taking the shape of the desired collector without using fasteners. The polyurethane foam is composed of two components (A and B) which are mixed in a 50:50 ratio and has a reaction time of 20 s to expand, while the drying time varies from 4 to 6 hours depending on the temperature and density of the components. 60 mL of each resin was used to cover the volume of the container enough to press the sheet against the mold.

2.4   Compound Parabolic Concentrator construction

Fig. 2 shows the manufacturing process. The flat surface of the 3D printed mold is placed inside the container, in such a way that remains in contact with the bottom of the mold recipient (Fig. 2a). Subsequently, the aluminum sheet is placed on the mold (previously cut according to the calculated area of the CPC design) thus adjusting to the parabolic design (Fig. 2b). Once the sheet and mold are inside the container, the A-B polyurethane foam mixture is added and immediately, the container is closed (Fig. 2c). As a chemical reaction result of the A-B polyurethane mixture, it turns into a foam that expands, generating pressure on the anodized aluminum sheet against the mold, acquiring the CPC profile (Fig. 2d). Finally, the lid of the container is removed, and the mold is separated from the collector. In this way, a sheet with the involute-shape made with a polyurethane foam base is obtained (Fig. 2e).
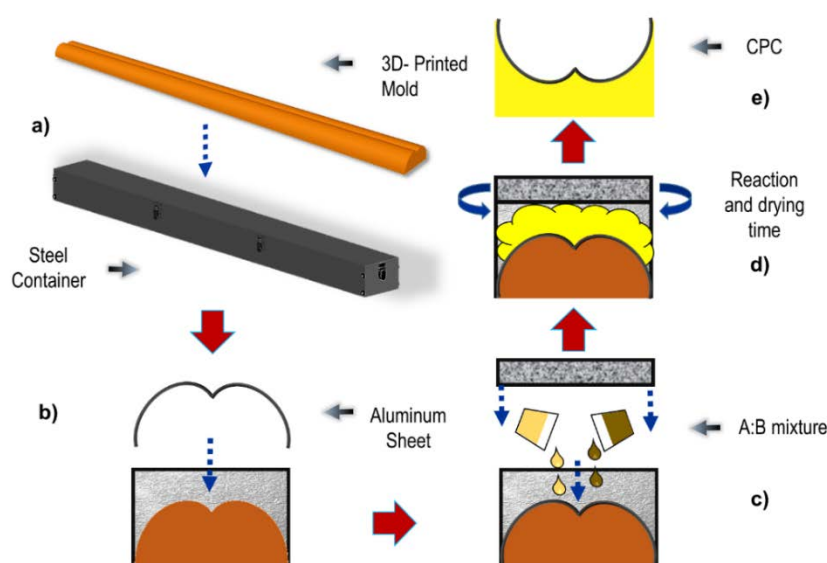

Fig. 2. CPC manufacturing process. a) the 3D-printed mold is introduced into the container, b) the anodized aluminum sheet is placed on top of the mold, c) the polyurethane foam mixture is poured, d) immediately closed where takes place the reaction and drying time and then e) the CPC is completed.

2.5   Evaluation of the CPC efficiency

A photogrammetry method was developed in order to validate the optical performance of the fabricated CPC and to evaluate the imperfections in the CPC sheet surface by machining or mechanical stress. As is illustrated in Fig. 3,

Journal of Applied Engineering Science

Vol. 20, No. 4, 2022

www.engineeringscience.rs

iipp

publishing

Pedro R. Martínez-Manuel et al. – Optical evaluation of 3D printed CPC by coupling photogrammetry and ray tracing analysis

the method consists of performing a three-dimensional surface reconstruction by photographs taken to the object under study. The modeling of the images obtained from the CPC was carried out through the software Caesoft® (v. 2016.0.5.1718). The technique was performed using a 2 mm dot pattern (Fig.3a) printed on vinyl with 5 mm separation between each dot, previously defined by the software itself; according to the camera calibration performance, where angles and location were processed and those photographs who were out of calibration were removed by the software itself. The dot pattern was placed on the entire surface to model (Fig. 3b), so that the points follow the shape of the CPC (Fig. 3c). After that, pictures from different positions around the pattern were taken with a Nikon® D3000 camera equipped with AF-S Nikkor 18-55 mm lens. Afterwards, the images obtained were processed and analyzed by Photomodeler software [24].
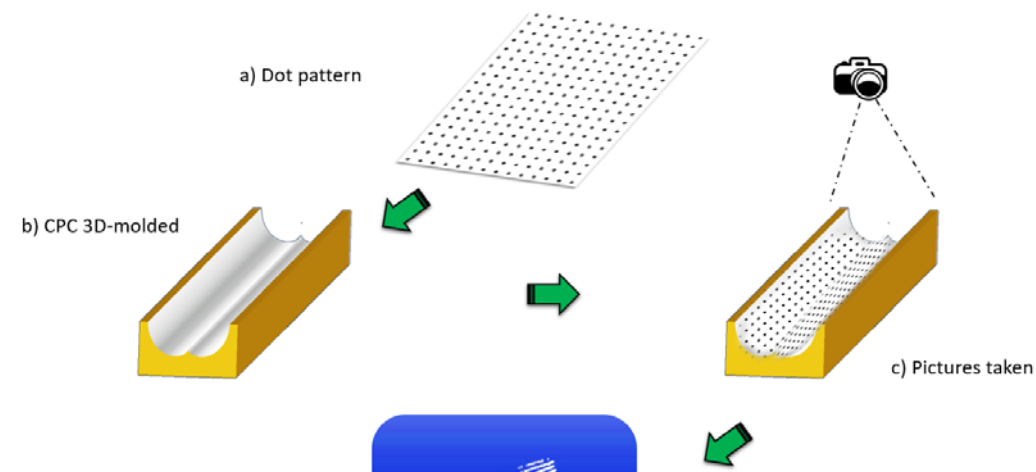

Fig. 3. Photogrammetry technique: a) 2 mm diameter dot pattern placed over the b) CPC 3D-molded and instantly c) a series of pictures are taken to process in PhotoModeler software and thus d) a point cloud is generated.

2.6   Analysis

Three types of evaluations were made in order to characterize and analyze both 3DM-CPC and CM-CPC: 1) a photogrammetric evaluation using a mathematical algorithm, 2) a Monte Carlo ray trace analysis of the structure based on the obtained data and 3) thermal energy generated by a water heating system simulated with SAM software.

The closest dot algorithm was used to evaluate the CPC-3D-surface of each CPC elaborated (3DM-CPC and CM-CPC) and thus compare it with an ideal design of a CPC of 1 sun geometric concentration (Fig. 1). This mathematical evaluation uses the dots array in x, y and z axis given by the PhotoModeler software and group the closest dots into clusters. The algorithm begins with an arbitrary starting data point. The neighborhood of this point is extracted using a distance (reference, in this case the 1-sun ideal CPC shape), if there are enough points within this neighborhood then the clustering process starts and the current data point becomes the first point of the new cluster. Otherwise, the point will be labeled as noise. For this first point in the new cluster, the points within a given ε distance neighborhood also become part of the same cluster. This procedure of making all points in the ε neighborhood belong to the same cluster is then repeated for all the new points that have been just added to the cluster group. After all dots are assigned, the centroids in the clusters are fixed. Finally, the closest clusters' centroids are compared to the 1-sun ideal CPC-reference[12]. These results are presented in the Fig. 5.

2.7   Evaluation with Ray Tracing software

To the closest point algorithm procedure, another workable assessment proposal with the data obtained is an advanced ray tracing study. The PhotoModeler software produces a 3D surface layer model (Fig. 4b) using the dot pattern of the images obtained according to the actual size of the 1-Sun CPC Collector (Fig. 4a). Afterwards, a .STL file is generated in PhotoModeler and exported to the design software AutoCAD®. In order to provide a real size and so manipulate it in Tonatiuh software, a pretreatment in AutoCAD® was made to the layer model (Fig. 4c) where a 5 mm thickness given to the surface, an aluminum solid material and a refined mesh model was assigned to the collector layer surface. Refinement of the surface mesh helps to mold smaller sections with less effect on the overall shape of the model. A mesh model comprises vertices, edges, and faces that use polygonal representation and it's applied to define a 3D shape model.
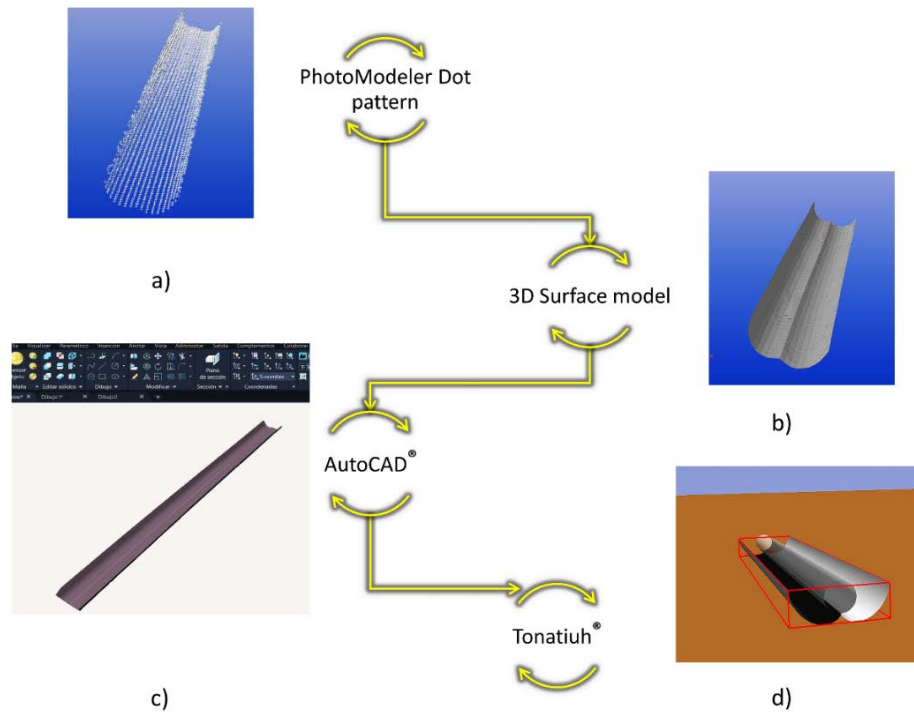
Fig. 4. Scheme showing the processing of the dot pattern obtained in PhotoModeler trough the AutoCAD software and so finally simulate the ray trace model in Tonatiuh.

Subsequently, a file with extension. STL of the model was generated, which can be exported to be used with Tonatiuh® software (v. 2.2.4). This software is a Monte Carlo ray tracer for optical simulation of solar concentration systems. Parameters such as incident solar power, minimum, maximum and average flux, uniformity and centroid location are visualized in the Tonatiuh environment. The described evaluation procedure based on the simulation of the optical performance allows to compare the irradiance collection efficiency of the three 1-sun CPCs under study; ideal CPC, 3D-molded (3DM-CPC) and the conventionally manufactured (CM-CPC). For this study, a 21.00 latitude and -102.00 longitude sun position and an inclination of the collectors of 21° were included as simulation parameters. Absorbance in the receiver tube of 96% and a reflectance of 95% were established as optical parameters according to the standard material specification.

The software flux distribution utility divides the selected surface according to a bi-dimensional regular grid of equal area cells. The number of grid divisions in the width (I) and length (J) dimensions are defined by the user. For flat surfaces, the grid applies to the smallest rectangle enclosing the surface. Since in local coordinates, a flat surface always lies in the y=0 plane, the 3D impact position of photons hitting the 3D flat surface is transformed to the 2D rectangular grid following the transformation:

$$(u, v) = (x, z) \qquad (6)$$

For cylindrical surfaces, the grid applies to the rectangle resulting from the unraveled surface of the cylinder starting from its generatrix. In local coordinates, the cylinder lies in the _xy_ plane with its axis parallel to the _z_-axis. Thus, a photon hit point at the 2D rectangular grid is given by a suitable transformation of its 3D impact position (_x,y,z_):

$$(u, v) = (r \cdot Atan2(x, y), z) \qquad (7)$$

Where _r_ is the cylinder radius and arctan2 is the two-argument arctangent function. It is then possible to count the number of photons intersecting each grid cell. With this knowledge the flux distribution and other related statistics can be computed. The radiative flux incident on a grid cell (i,j) is:

$$\Phi_{i,j} = \frac{N_{i,j} P_{ph}}{A_c} \qquad (8)$$

Where $N_{i,j}$ is the number of photons intersecting the grid cell (i,j), P_{ph} is the power carried by each photon and A_c denotes the grid cell area. The total incident power on the surface is given by:

$$\dot{Q} = P_{ph} \sum_{i=1}^{I} \sum_{j=1}^{J} N_{i,j} \qquad (9)$$

The average radiative flux in the surface is given by:

Journal of Applied Engineering Science

Vol. 20, No. 4, 2022

www.engineeringscience.rs

iipp
publishing

Pedro R. Martínez-Manuel et al. – Optical evaluation of 3D printed CPC by coupling photogrammetry and ray tracing analysis

$$\overline{\Phi} = \frac{P_{ph} \sum_{i=1}^{I} \sum_{j=1}^{J} \Phi_{i,j}}{IJ} \tag{10}$$

2.8 Evaluation of thermal efficiency

In order to estimate the impact on the thermal energy generated by a water heating system with the CPCs under study, SAM software was used [25]. SAM applies the Hottel-Whillier-Bliss (equation 11) to express the thermal performance of a collector under steady state. This equation to estimates the useful gain by the solar heating system as follows:

$$Q_u = A \cdot \left[\eta_{opt} \cdot FR\tau\alpha \cdot \kappa_{\tau\alpha}(\theta_b) \cdot G_I - FRU_L(T_i - T_{amb}) \right] \tag{11}$$

Where:

Q_u - Solar field useful gain (kW)

A- Total system collector area (m²)

$\eta_{opt} \cdot FR\tau\alpha$ - Optical gain

$\kappa_{\tau\alpha}(\theta_b)$ - Modifier at AM 1.5

G_I- Incident solar irradiance normal to the collector plane W m⁻²

FRU_L- Thermal loss coefficient

T_i- Solar field inlet temperature of the working fluid

T_∞- Dry bulb temperature

Optical gain factor ($FR\tau\alpha$) in SAM software was assumed as a function of the average CPC optical efficiency calculated by ray tracing in this work (η_{opt}) as shown in Table 1.

Table 1. Relative optical gain in Hottel-Whillier-Bliss (equation 11) as a function of the CPC optical efficiency.

Type	Average optical efficiency $\boldsymbol{\eta_{opt}}$	Coef. $\boldsymbol{\eta_{opt} \cdot FR\tau\alpha}$
Ideal CPC	1	0.607
3DM - CPC	0.95	0.57665
CM - CPC	0.82	0.49774

The main parameters considered in the SAM simulation were:

Table 2. Parameters of the simulated solar water heating system

Parameter	Value
Location	Aguascalientes, México (21.88° lat, -102.296° lon)
Average hot water usage	1000 L/day⁻¹
Collector tilt angle	22 °
Total system flow rate	0.83 kg/s⁻¹
Working fluid	Water
No. of Collectors	15
Collector Area	2.78 m²
FRta	0.607, 0.57665, 0.49774
FRUL	3.72 W/m⁻² °C
Incident angle modifier	0.95
Test fluid	Glycol
Test flow	0.0556 kg/s⁻¹
Solar tank volume	1000 L
Outlet set temperature	80 °C

3 RESULTS

3.1 closest dot algorithm

The Fig. 5a (up-left) shows the CPC 3D mold data (blue dots) and its mean absolute error (down-left) acquired by using the photogrammetry technique and represented in a single plane comparing to the ideal geometric 1-sun CPC

shape (red dots line) elaborated in Matlab software in accordance with equations 1-5. Likewise, the Fig.5b exhibits the comparison of the CM-CPC (up-right) specifying its mean absolute error (down-right), in which construction techniques such as bending, punching and manual bending were used. The 3DM-CPC mean deviation stated in the Fig. 5a is barely 1.2 mm which is a remarkable, since a novel and cheap procedure was followed according to the manufacturing method shown in Fig. 3. This proves that the proposed manufacturing technique using a 3D mold and polyurethane foam is adequate and considerably better approximated to the ideal shape of the analyzed CPC.

On the other hand, the results show a major mean deviation of the CM-CPC with a 3.19 mm error. As shown in Fig. 5b the curved shape of the involute was not achieved specially at the CPC edges, it can be attributed to the less precise hand-made manufacture technique.
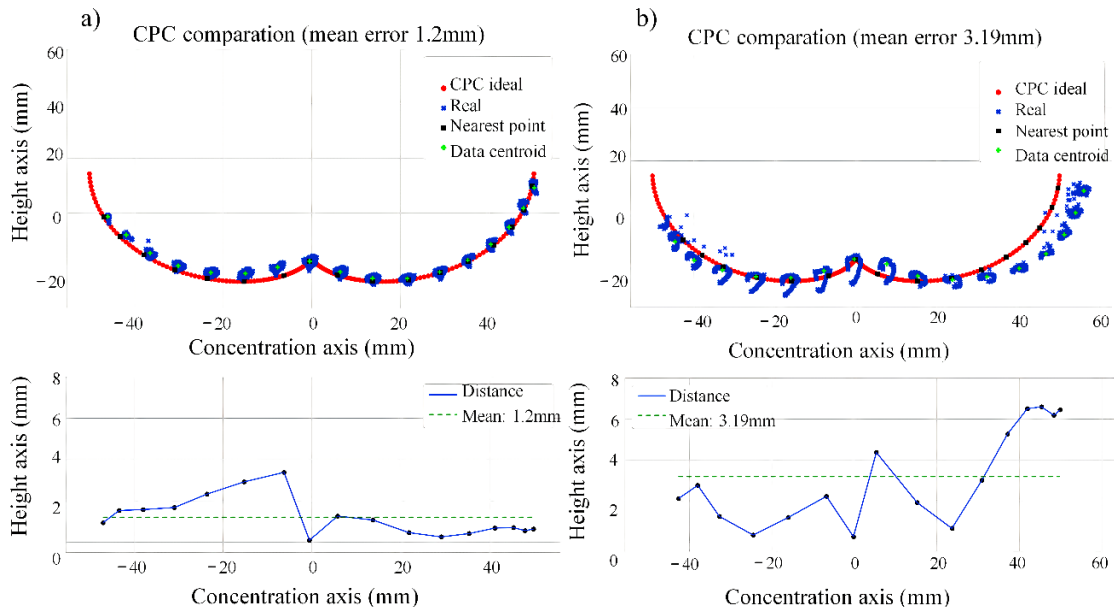

Fig. 5. Graphs showing the ideal 1-sun-CPC (red dotted line), compared to the 3D-mold technique 3DM-CPC (a) and the cconventionally manufactured CM-CPC (b) and their mean error in mm, respectively (below).

Regardless of the mean absolute error (MAE) in the 3DM-CPC according to its dimensions and shape, it becomes negligible. This MAE can be attributed to two causes, 1) the length of the CPC (1300 mm) which is considerably large and 2) the data centroids, that is a high data number given by the software itself. This is because of the dots pattern is very close from one point to another (5 mm) for an optimal surface scan, moreover the CPC shape is very curved on its edges because of its parabolic form, which makes it difficult for the software to process the images. It should be noted, however, that there is an inherent uncertainty in the data collected by the photogrammetric technique, which is attributed to different factors that determine the accuracy of a photogrammetric analysis. The key factors affecting accuracy are photo resolution, camera calibration, angles, photo orientation, quality photo redundancy and targets/marking precision. Aspects like focal length, distortion lens, number of pixels, angled photos for more detail, number of photos, target size and software precision marking targets by pixel are some examples of them.

An estimation of the root mean square standard error (RMSE) was calculated using the data collected by the PhotoModeler software that provides a set of residual points in pixels from the 3D surface layer model. The RMSE value calculated is ±0.01 px or 0.002 mm. Thus, a general projected error data is considered for the reported result.

3.2   Result of ray tracing analysis

Using Tonatiuh® software, a Monte Carlo ray trace studio was simulated for the three surface models in the same solar conditions (angle, position, location) in order to evaluate the concentrating performance. Fig. 6 shows the ray trace simulation for a 21.00 latitude and -102.00 longitude sun position to compare the ideal CPC, the 3DM-CPC and the CM-CPC.
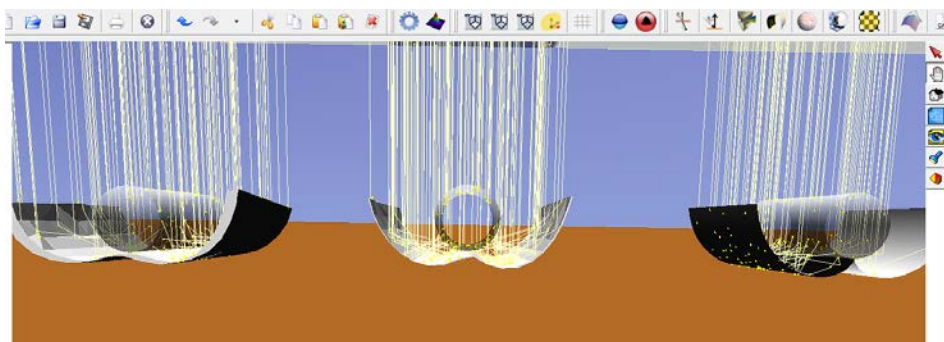

Fig. 6. Ray trace simulation environment for all CPC configurations: ideal (right), 3DM-CPC (center) and CM-CPC (left).

Journal of Applied Engineering Science

Vol. 20, No. 4, 2022

www.engineeringscience.rs

iipp
publishing

Pedro R. Martínez-Manuel et al. – Optical evaluation of 3D printed CPC by coupling photogrammetry and ray tracing analysis

The ray tracing studio consists in estimate the four-day seasons positions (solstices and equinoxes) to show and compare the 3DM-CPC and the CM-CPC functionality and efficiency against the 1-sun ideal collector, measuring hourly during 9 hours (9:00 am – 6:00 pm) the simulated incident radiative flux collected in the receptor tube during each of the four days (vernal equinox, summer solstice, autumnal equinox and winter solstice), the results are shown in Fig.7.
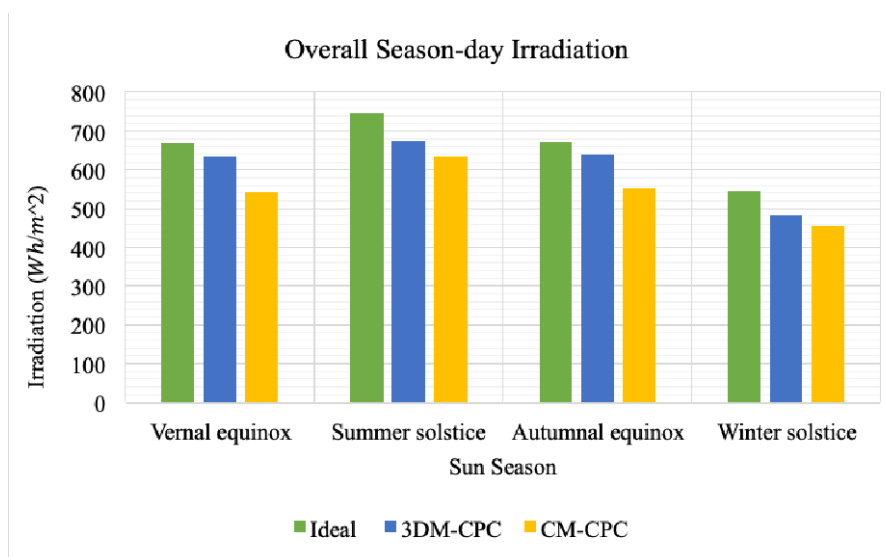

Fig. 7. Shows the irradiances performances of the ideal 1-sun-CPC, 3DM-CPC and CM-CPC for the four sun seasons; vernal equinox (March 21), summer solstice (June 21), autumnal equinox (September 23) and winter solstice (December 23).

The results presented in Fig. 7 show the overall season-day sun irradiation for the four dates in every collector based on the integrated irradiation. The collecting performance of the 3DM-CPC and the CM-CPC are compared with the ideal 1-sun CPC using the results of the area under the curve related to the simulated irradiance along each day for each collector.

As can be seen in Fig. 7, the difference between a CM-CPC and a 3DM-CPC is relevant, the 3DM-CPC showed a higher solar collection efficiency factor than the CM-CPC. Assuming that the ideal 1-Sun collector has the 100% percent efficiency factor, the 3DM-CPC and the CM-CPC obtain a 95 % max – 88 % min and an 85% max – 81% min range, respectively. Although 3DM-CPC has some errors in the reflective surface, it is close to its shape because of the presented manufacturing technique. This allows 3DM-CPC to have a considerably better performance than the CM-CPC built from mechanical shaping techniques and tools. The graphs in Fig. 7 confirms the performance difference according to the manufacturing technique respect to the ideal one, being this the most efficient on the four graphs, followed by the one with the 3DM-CPC and lastly the CM-CPC collector shape.

3.3 Result of thermal energy generated

In order to validate the benefits of the different CPCs, the study was complemented by a thermal energy performance analysis of a simulated 1000 L CPC solar plant with 15 collectors and 2.78 m^2 of total area (full parameters are shown in table 2). Fig. 8 shows the thermal energy in kWh generated throughout a year comparing the 3 different CPCs under study. In all the months evaluated, the difference of thermal energy generated by using 3DM-CPC compared with CM-CPC is significant, achieving improvements up to 13% in December. It is important to notice that the performance of the 3DM-CPC collector is, in most cases, similar to the ideal-CPC. The smallest difference between the thermal energy generated by a solar plant modelled with a 3DM-CPC and the hypothetical ideal case is only 1%, evaluated by the SAM software in the months of April and October. As can be seen in table 3, in one year a benefit of 1,631 kWh (≈9.4%) could be obtained, represented by the better reflective quality of the 3DM-CPC in which the surface of the aluminum sheet suffers less damage

Table 3. Summary - thermal energy generated by the system

	CPC Solar Manufacture type		
	Ideal CPC	3DM- CPC	CM – CPC
Annual thermal energy generated [kWh]	19 440.73	19 016.18	17 384.96

.

Journal of Applied Engineering Science

Vol. 20, No. 4, 2022

www.engineeringscience.rs

iipp
publishing

Pedro R. Martínez-Manuel et al. - Optical evaluation of 3D printed CPC by coupling photogrammetry and ray tracing analysis
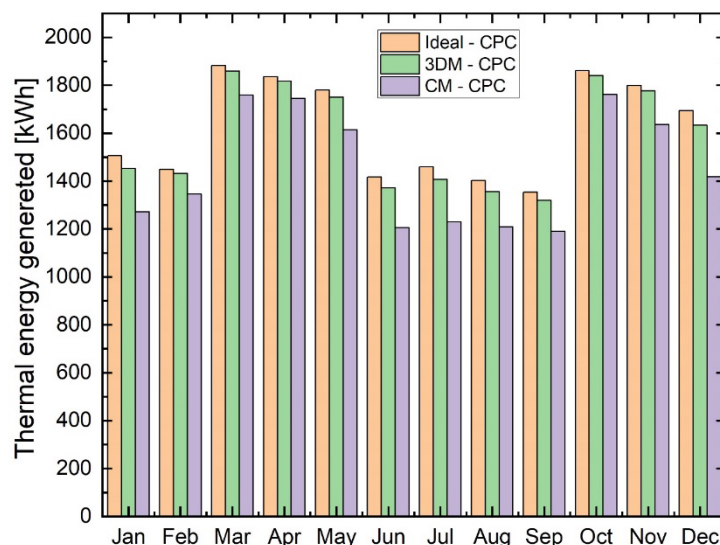
Fig. 8. Monthly thermal energy generated by the solar water heating system.

4 CONCLUSION

In the presented work a manufacturing process to fabricate a CPC with the aid of a 3D printed mold and polyurethane foam (3DM-CPC) is proposed and is compared to a conventionally manufactured CPC (CM-CPC) in reference to an ideal 1-sun concentration system. An alternative method for the optical evaluation of CPC collectors using ray tracing analysis in a 3D model generated by inverse engineering is also proposed. With this novel evaluation procedure, the optical performance of both the 3DM-CPC and CM-CPC CPCs were evaluated through a photogrammetric optical procedure and analyzed by a closest point mathematical algorithm. The results in manufacturing efficiency gives a MAE of 1.2 and 3.19 for the 3DM-CPC and the CM-CPC, respectively. A Monte Carlo ray tracing evaluation was made to support the collector shape assessment, where a four-day sun positions analysis shows under different irradiation conditions the overall performance and effectiveness of the 3DM-CPC and CM-CPC collectors. Showing that in everyday the 3DM-CPC collector obtained a better efficiency than the CM-CPC, where a 95% efficiency on the 3DM-CPC was reached against the 82% efficiency of the CM-CPC in the autumnal equinox day i.e., both compared to the ideal 1-sun-CPC collector (100% efficiency factor). Even though the low irradiance contribution in the case of the winter solstice, the 3DM-CPC shows the best irradiation collecting results. Both results reiterate the advantage and effectiveness of the proposed manufacturing method. This assessment infers a determinant factor in solar collector's optical performance, especially in low-power concentration because the limited UV solar radiation available, e.g. for chemical processes. The improvements in the presented CPC manufacturing process are verified by studying the performance of a Solar CPC Thermal Plant using the SAM software. Yield improves considerably, up to a maximum of 13% in December evaluation. The benefit could be 1,631 kWh (≈9.4%) in the annual performance of the plant with the improved CPCs.

5 ACKNOWLEDGMENTS

6 REFERENCES

[1] Tian, M., Su, Y., Zheng, H., Pei, G., Li, G., Riffat, S. (2018). A review on the recent research progress in the compound parabolic concentrator (CPC) for solar energy applications. Renewable and Sustainable Energy Reviews, vol. 82, no. October 2017, 1272–1296. DOI:10.1016/j.rser.2017.09.050

[2] Jaaz, A. H., Hasan, H. A., Sopian, K., Haji Ruslan, M. H. Bin, Zaidi, S. H. (2017). Design and development of compound parabolic concentrating for photovoltaic solar collector: Review. Renewable and Sustainable Energy Reviews, vol. 76, 1108–1121. DOI:10.1016/J.RSER.2017.03.127

[3] Santos-González, I., García-Valladares, O., Ortega, N., Gómez, V. H. (2017). Numerical Modeling and Experimental Analysis of the Thermal Performance of a Compound Parabolic Concentrator, Applied Thermal Engineering, vol. 114. DOI:10.1016/j.applthermaleng.2016.10.100

Journal of Applied Engineering Science

Vol. 20, No. 4, 2022

www.engineeringscience.rs

iipp publishing

Pedro R. Martínez-Manuel et al. – Optical evaluation of 3D printed CPC by coupling photogrammetry and ray tracing analysis

[4] Mishra, R. K., Garg, V., Tiwari, G. N. (2017). Energy matrices of U-shaped evacuated tubular collector (ETC) integrated with compound parabolic concentrator (CPC). Solar Energy, vol. 153, 531–539. DOI:10.1016/J.SOLENER.2017.06.004

[5] Yin, P., Lv, J., Wang, X., Huang, R. (2021). A spectral splitting planar solar concentrator with a linear compound parabolic lightguide for optical fiber daylighting. Renewable Energy, vol. 179, 778–787. DOI:10.1016/j.renene.2021.07.100

[6] McMichael, S., Waso, M., Reyneke, B., Khan, W., Byrne, J. A., Fernandez-Ibanez, P. (2021). Electrochemically assisted photocatalysis for the disinfection of rainwater under solar irradiation. Applied Catalysis B: Environmental, vol. 281, no. August 2020, 119485. DOI:10.1016/j.apcatb.2020.119485

[7] Cabrera-Reina, A., Miralles-Cuevas, S., Rivas, G., Sánchez Pérez, J. A. (2019). Comparison of different detoxification pilot plants for the treatment of industrial wastewater by solar photo-Fenton: Are raceway pond reactors a feasible option?. Science of the Total Environment, vol. 648, 601–608. DOI:10.1016/j.scitotenv.2018.08.143

[8] Tiwari, D., Sherwani, A. F., Atheaya, D., Arora, A. (2017). Energy and exergy analysis of solar driven recuperated organic Rankine cycle using glazed reverse absorber conventional compound parabolic concentrator (GRACCPC) system. Solar Energy, vol. 155, 1431–1442. DOI:10.1016/J.SOLENER.2017.08.001

[9] Elashmawy, M. (2017). An experimental investigation of a parabolic concentrator solar tracking system integrated with a tubular solar still. Desalination, vol. 411, 1–8. DOI:10.1016/J.DESAL.2017.02.003

[10] Moreno-SanSegundo, J., Martín-Sómer, M., Marugán, J. (2022). Dynamic concentration factor: A novel parameter for the rigorous evaluation of solar compound parabolic collectors. Chemical Engineering Journal, vol. 437, no. December 2021. DOI:10.1016/j.cej.2022.135360

[11] Fendrich, M. A., Quaranta, A., Orlandi, M., Bettonte, M., Miotello, A. (2018). Solar concentration for wastewaters remediation: A review of materials and technologies. Applied Sciences, vol. 9, no. 1. DOI:10.3390/app9010118

[12] Carrillo, J. G., Peña-Cruz, M., Terrón-Hernández, M., Valentin, L. (2020). Low Cost High-Accuracy CPC System - A Manufacturing Methodology. Journal of Solar Energy Engineering, 1–13. DOI:10.1115/1.4048015

[13] Chafie, M., Ben Aissa, M. F., Bouadila, S., Balghouthi, M., Farhat, A., Guizani, A. (2016). Experimental investigation of parabolic trough collector system under Tunisian climate: Design, manufacturing and performance assessment. Applied Thermal Engineering. DOI:10.1016/j.applthermaleng.2016.02.073

[14] Forman, P., Müller, S., Ahrens, M. A., Schnell, J., Mark, P., Höffer, R., Hennecke, K., Krüger, J. (2015). Light concrete shells for parabolic trough collectors - Conceptual design, prototype and proof of accuracy. Solar Energy, vol. 111, 364–377. DOI:10.1016/j.solener.2014.11.002

[15] Meiser, S., Schneider, S., Lüpfert, E., Schiricke, B., Pitz-Paal, R. (2017). Evaluation and assessment of gravity load on mirror shape and focusing quality of parabolic trough solar mirrors using finite-element analysis. Applied Energy. DOI:10.1016/j.apenergy.2016.04.045

[16] Balghouthi, M., Ali, A. B. H., Trabelsi, S. E., Guizani, A. (2014). Optical and thermal evaluations of a medium temperature parabolic trough solar collector used in a cooling installation. Energy Conversion and Management. DOI:10.1016/j.enconman.2014.06.095

[17] Osório, T., Horta, P., Collares-Pereira, M. (2019). Method for customized design of a quasi-stationary CPC-type solar collector to minimize the energy cost. Renewable Energy, vol. 133, 1086–1098. DOI:10.1016/J.RENENE.2018.10.110

[18] Jadhav, A. S., Gudekar, A. S., Patil, R. G., Kale, D. M., Panse, S. V., Joshi, J. B. (2013). Performance analysis of a novel and cost effective CPC system. Energy Conversion and Management, vol. 66, 56–65. DOI:10.1016/J.ENCONMAN.2012.09.030

[19] El Ydrissi, M., Ghennioui, H., Bennouna, E. G., Farid, A. (2019). A review of optical errors and available applications of deflectometry technique in solar thermal power applications. Renewable and Sustainable Energy Reviews, vol. 116, no. October, 109438. DOI:10.1016/j.rser.2019.109438

[20] El Ydrissi, M., Ghennioui, H., Bennouna, E. G., Farid, A. (2019). Geometric, optical and thermal analysis for solar parabolic trough concentrator efficiency improvement using the photogrammetry technique under semi-arid climate. Energy Procedia, vol. 157, no. 2018, 1050–1060. DOI:10.1016/j.egypro.2018.11.272

[21] Waghmare, S. A., Gulhane, N. P. (2017). Optical evaluation of compound parabolic collector with low acceptance angle. Optik, vol. 149, 359–371. DOI:10.1016/J.IJLEO.2017.09.039

[22] Lara, F., Cerezo, J., Acuña, A., González-Ángeles, A., Velázquez, N., Ruelas, A., López-Zavala, R. (2021). Design, optimization and comparative study of a solar CPC with a fully illuminated tubular receiver and a fin inverted V-shaped receiver. Applied Thermal Engineering, vol. 184, 116141. DOI:10.1016/J.APPLTHERMALENG.2020.116141

[23] Salgado-Tránsito, I., Jiménez-González, A. E., Ramón-García, M. L., Pineda-Arellano, C. A., Estrada-Gasca, C. A. (2015). Design of a novel CPC collector for the photodegradation of carbaryl pesticides as a function of the solar concentration ratio. Solar Energy, vol. 115, 537–551. DOI:10.1016/j.solener.2015.02.034

[24] King, P., Sansom, C., Comley, P. (2020). Photogrammetry for concentrating solar collector form measurement, validated using a coordinate measuring machine. Sustainability, vol. 12, no. 1, 1–20. DOI:10.3390/su12010196

[25] Li, X., Jin, J., Yang, D., Xu, N., Wang, Y., Mi, X. (2019). Comparison of tower and trough solar thermal power plant efficiencies in different regions of China based on SAM simulation. AIP Conference Proceedings, vol. 2126, no. July. DOI:10.1063/1.5117545